Application of the wavelet transforms on axial strain calculation in ultrasound elastography[*]

LUO Jianwen, BAI Jing[**] and SHAO Jinhua

(Department of Biomedical Engineering, School of Medicine, Tsinghua University, Beijing 100084, China)

Abstract   In ultrasound elastography, the axial strain distribution within biological tissues is calculated as the numerical derivative (differentiation) of the estimated axial displacement field. Unfortunately, the numerical derivative is unstable because it can greatly amplify the noises, especially at high frequencies. This work focuses on the axial strain calculation from the estimated axial displacements using wavelet transforms (WTs), including continuous wavelet transforms (CWTs) and discrete wavelet transforms (DWTs). The feasibility of the WT-based method using the quadratic spline function is verified by computer simulations and some phantom data. Results indicate that the WT-based method can effectively reduce the noise amplification in axial strain calculation.

Keywords: ultrasound, elastography, axial strain, differentiation, wavelet transforms.

Ultrasound elastography has become a promising method for quantifying and imaging the elastic properties of biological tissues[1—3]. In ultrasound elastography with a static or quasi-static compression, tissue axial strains are calculated from the derivative of the estimated axial displacements with respect to space[1—3]. However, the common differentiation operation amplifies the noises in the displacement estimation, especially at high frequencies[4, 5]. Researchers have proposed different methods to reduce the noise of the strain image, e. g. the combination of the low-pass filter or moving average filter and the derivative formula[2, 6], the least-squares strain estimator (LSQSE)[6] and the method of the low-pass digital differentiator (LPDD)[7]. A strain estimator based on wavelet transform was also proposed[8]. Similar to adaptive stretching strain estimator[9], it uses the scale factor maximizing the wavelet transfer function to calculate the strain. Though this method is effective, it is time consuming[8].

In this work, a new method based on wavelet transforms (WTs)[10, 11], including continuous wavelet transforms (CWTs) and discrete wavelet transforms (DWTs), is proposed for axial strain calculation in elastography. It is known that the WT with a wavelet function having no more than n vanishing moments is a multiscale differential operator[10—14]. According to this property, the local extrema (modulus maxima) or zero crossings of the first and second derivatives are widely used for singularity detection (e. g. edge detection) and characterization of a signal[12—16]. Recently, both the CWTs and DWTs were applied to approximate derivative calculation in analytical chemistry and chemometrics[17—22]. The WT-based derivative calculation has also been applied to discrete vibrational data for detecting open cracks in damaged beams[23, 24], and to derivative analysis of hyperspectral signatures for computing scale-space images and spectral fingerprints[25]. Using the Mallat's algorithm[10, 11] or the A'trous algorithm[10, 11], the DWT-based method has the advantage of high computational efficiency[25].

In this work, the quadratic spline function (i. e. the derivative of the cubic spline function)[15, 19] is used as the wavelet function. The corresponding CWTs and DWTs are used to calculate the axial strains from the estimated axial displacements in ultrasound elastography. Results of computer simulations and phantom data processing show that the CWTs and the DWTs have the properties of both denoising and differentiation.

1　Theory

1.1　CWT-based differentiation method

The CWT of a signal $y(x)$ is defined as[10, 11, 24]

$$y(\bar{x})^{\text{w}} = \int_{-\infty}^{+\infty} y(x)\frac{1}{\sqrt{s}}\psi\left(\frac{x-\bar{x}}{s}\right)\mathrm{d}x, \qquad (1)$$

where s and $\bar{x}$ are the dilation parameter and translation parameter, respectively; $\psi(x)$ is a finite energy function having a zero average called mother wavelet, basic wavelet or wavelet function.

Consider a wavelet function $\psi(x)$ defined by the derivative of a smoothing function $\theta(x)$ plus a minus. The smoothing function $\theta(x)$ has a fast decay and a nonzero constant integral as[10,24]

$$\int_{-\infty}^{+\infty} \theta(x)\mathrm{d}x = \Theta(\omega)\mid_{\omega=0} = K \neq 0, \qquad (2)$$

where $\Theta(\omega)$ is the Fourier transform of $\theta(x)$. Eq. (2) also establishes that $\psi(x)$ has no more than one vanishing moment[10,24].

It has been proved that the CWT $y(\bar{x})^{\text{w}}$ with the above wavelet function is just the derivative of the signal $y(x)$ smoothed by a weighted average kernel $\theta_s(x)$, which corresponds to the smoothing function $\theta(x)$ dilated through s, weighted through $\frac{1}{\sqrt{s}}$ and turned over through $-x$[10,24]. As a result, the CWT with the given wavelet function $\psi(x)$ has the combined properties of data smoothing and differentiation. In particular, one can verify that[10,24]

$$\lim_{s\to 0}\frac{y(\bar{x})^{\text{w}}}{Ks^{3/2}} = \frac{\mathrm{d}y(x)}{\mathrm{d}x}. \qquad (3)$$

According to Eq. (3), it is natural to use $\frac{y(\bar{x})^{\text{w}}}{Ks^{3/2}}$ to approximate the derivative. A small value of the dilation parameter results in high noise sensitivity, while a large value of the dilation parameter is related to a large averaging domain and hence results in strong noise cancellation.

The frequency response of the above-mentioned method can be derived as[24]

$$H(\omega) = \frac{Y(\omega;s)^{\text{w}}}{Ks^{3/2}\cdot Y(\omega)} = \frac{\mathrm{j}\omega\Theta(-s\omega)}{K}, \qquad (4)$$

where $Y(\omega)$ and $Y(\omega;s)^{\text{w}}$ are the Fourier transforms of $y(x)$ and $y(\bar{x})^{\text{w}}$, respectively; $\mathrm{j}\omega$ represents the frequency response of an ideal differentiator.

Furthermore, the tangent of the frequency response at the low frequency $\omega=0$ satisfies

$$H'(\omega)\mid_{\omega=0} = \frac{\mathrm{j}\Theta(-s\omega)\mid_{\omega=0}}{K} = \mathrm{j}. \qquad (5)$$

As a consequence, the frequency response approaches the ideal differentiator at low frequencies.

1.2   DWT-based differentiation method

The DWTs can also be used to calculate the approximate derivative[17,22,25]. Results indicated that both the CWTs and DWTs showed similar characteristics with a given wavelet function[21]. Moreover, the DWT has an efficient fast algorithm with the multiresolution analysis, i. e. the Mallat's algorithm[10,11]. To avoid data subsampling (decimation), the A' trous algorithm[10,11] is preferable. Similar to the CWT-based differentiation method, the DWT-based method uses $\frac{y(\bar{x})^{\text{dwt}}}{K2^{3n/2}}$ to approximate the derivative, where $y(\bar{x})^{\text{dwt}}$ is the DWT (i. e. wavelet coefficients or detail coefficients/information in the multiresolution signal decomposition[10,11]) of $y(x)$ on the signal decomposition level of n, and 2^n corresponds to dilation parameter s in the CWT method.

2   Method

2.1   Axial strain calculation

In the above theoretical analysis, the sampling interval is assumed to be unit. In ultrasound elastography, the sampling interval is equal to the window separation ΔW in the cross-correlation analysis for the axial displacement estimation. Considering this aspect, the axial strains $e(\bar{x})$ can be calculated from the estimated axial displacements using the CWT-based differentiation method using

$$e(\bar{x}) = \frac{u(\bar{x})^{\text{w}}}{Ks^{3/2}\Delta W}, \qquad (6)$$

where $u(\bar{x})^{\text{w}}$ is the CWT of the estimated axial displacements $u(x)$. The axial strain calculation using the DWT-based method is similar.

2.2   Boundary effect

Similar to the LPDDs[7], the WT-based differentiation has a boundary effect, i. e. the side-lobe problem[10,23,24]. The input signal (axial displacements) has a finite length, and so an apparent abrupt transient occurs at the data boundaries (i. e. initial and terminal points). The method of translation-rotation transformation (TRT)[17,22,26,27] eliminates this transient by subtracting a linear component from the input signal to reduce the boundary effect.

Before the calculation of CWT, the axial dis-

placements are processed with the TRT method by[27]

$$u^{\mathrm{TRT}}(x) = u(x) - [ax + b], \qquad (7)$$

where

$$a = \frac{u(x_{\max}) - u(x_{\min})}{x_{\max} - x_{\min}},$$

and

$$b = u(x_{\min}) - ax_{\min}.$$

Similar to Eq. (6), the derivative of $u^{\mathrm{TRT}}(x)$ is given by

$$e^{\mathrm{TRT}}(\bar{x}) = \frac{u_x^{\mathrm{TRT}}(\bar{x})^{\mathrm{w}}}{Ks^{3/2}\Delta W}, \qquad (8)$$

where $u_x^{\mathrm{TRT}}(\bar{x})^{\mathrm{w}}$ is the CWT of $u^{\mathrm{TRT}}(x)$.

The difference between $u^{\mathrm{TRT}}(x)$ and $u(x)$ is the linear component $ax + b$. Therefore, the difference between their derivative would be the derivative of $ax + b$, i.e. a. Finally, the axial strains are calculated by $u^{\mathrm{TRT}}(x)$ plus a, which is eliminated in the TRT method, i.e.

$$e(\bar{x}) = e^{\mathrm{TRT}}(\bar{x}) + a. \qquad (9)$$

When the DWT-based differentiation method is used, the term of s in Eq. (8) should be replaced by 2^n and the CWT $u_x^{\mathrm{TRT}}(\bar{x})^{\mathrm{w}}$ in Eqs. (8) and (9) should be replaced by the DWT $u_x^{\mathrm{TRT}}(\bar{x})^{\mathrm{dwt}}$.

3 Simulation

The same method and the single-lesion model used in our previous work[9] were utilized for Monte Carlo simulations. More details about the simulation methods and parameters can be seen in Ref. [9]. The axial displacements were estimated using a window length of 2 mm and a window separation of 0.5 mm (i.e. at a 75% overlap). Then, with the wavelet toolbox[28] in MATLAB 6.5 (The Math-Works Inc., Natick, MA), the CWT and DWT were applied to calculate the axial strains using the estimated axial displacements.

Fig. 1 compares the ideal strain image (top left), the strain image calculated by the commonly-used numerical derivative method (two-point formula) (top right), and the strain images calculated by the CWT method with different dilation parameters (bottom rows). All images correspond to a region of 50 mm × 50 mm. The vertical axis denotes the axial direction (depth), while the horizontal axis denotes the lateral direction (width). As can be seen qualitatively from Fig. 1, the strain variation of the strain images significantly decreases with the increasing dilation parameter. Therefore, the elastographic signal-to-noise ratio (SNRe)[7,29,30] is significantly improved. However, the improvement of the SNRe seems to be at the expense of a lower contrast and axial resolution (AR)[31,32]. Fig. 1 also shows the superiority of the CWT method over the conventional derivative method for axial strain calculation.
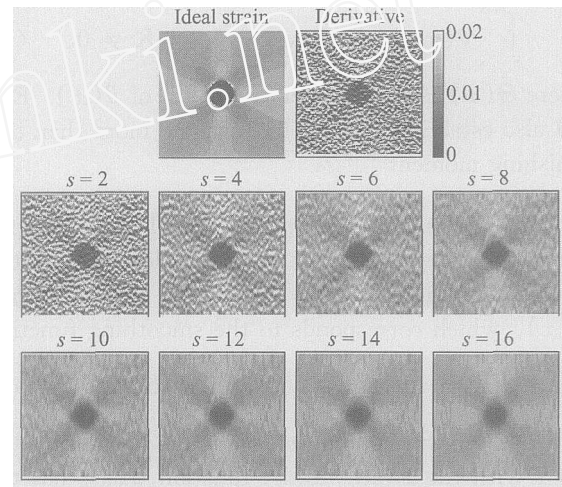

Fig. 1. The ideal strain images (top left), the strain image calculated by the common numerical derivative method (top right), and the strain images calculated by the CWT method (bottom rows) with different dilation parameters (s).

To compare the performances of different dilation parameters quantitatively, the elastographic contrast-to-noise ratio (CNRe)[29,33], which is ultimately related to the detectability of lesions, is calculated from the strain profiles along the central line of the tissue and shown in Fig. 2. The CNRe is defined as[5,29,33],

$$\mathrm{CNRe} = \frac{2(\mu_{s_b} - \mu_{s_l})^2}{\sigma_{s_b}^2 + \sigma_{s_l}^2}, \qquad (10)$$

where μ_{s_b} and μ_{s_l} represent the mean values of the strains in the background tissue and the lesion, while $\sigma_{s_b}^2$ and $\sigma_{s_l}^2$ denote the strain standard deviations in the background and the lesion, respectively. As can be seen in Fig. 2, the CNRe first increases with the dilation parameter, peaks at the dilation parameter of 9, and then decreases with its further increasing.

Fig. 3 presents the strain image calculated by the DWT method (with the A'trous algorithm) on different decomposition levels (n). The elastographic
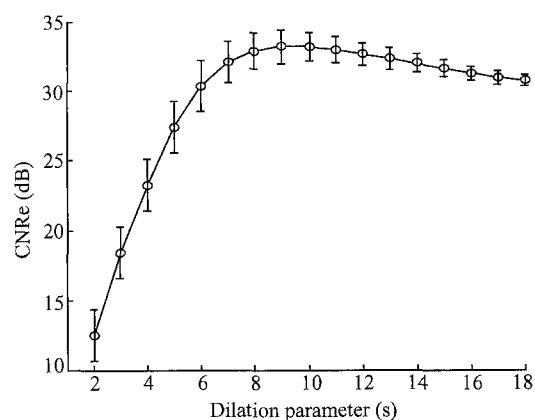
Fig. 2.   The CNRe of the strain profiles along the central line of the tissue obtained by the CWT method with different dilation parameters. The results are averaged over 50 independent realizations and plotted on a decibel (dB) scale; the error bars represent the standard deviations.

performances of the DWT method on different decomposition levels are similar to the performances of the CWT method with different dilation parameters. In particular, the performances of the DWT method on the decomposition levels of 1, 2, 3 and 4 are similar to those of the CWT method with the dilation parameters of 2, 4, 8 and 16, respectively.
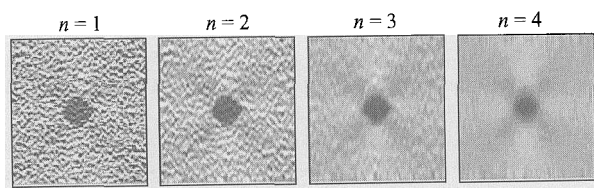

Fig. 3.   The strain image calculated by the DWT method on different decomposition levels (n).

4   Experiment

Due to the lack of suitable elastographic phantoms, some raw radio-frequency (RF) data (A-lines)[34] were taken from the University of Texas Medical School with their permission to validate the feasibility of the WT-based method for axial strain calculation. More details of the experimental setting and parameters can be seen in Ref. [34]. The axial displacements were estimated using a window length of 2 mm and a window separation of 0.5 mm (i.e. at a 75% overlap).

Fig. 4 shows the pre-compression sonogram of the phantom (top left) and the axial strain image calculated by the commonly-used derivate method (top right), as well as the strain images obtained by the CWT method with different dilation parameters. All images correspond to a region of 57 mm × 38 mm

(depth × width), and the vertical and horizontal axes denote the axial and lateral directions, respectively. The experimental performances with different dilation parameters in Fig. 4 are very similar to those of simulations.
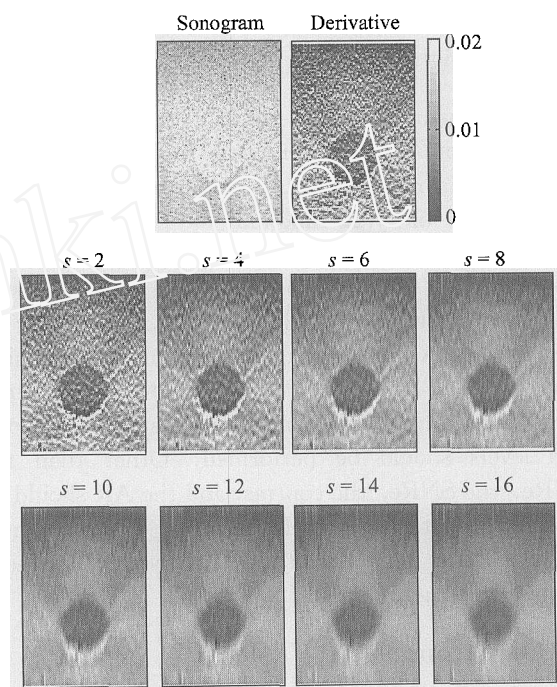

Fig. 4.   The pre-compression sonogram of the phantom (top left), the strain images calculated by the numerical derivative method (top right) and the strain images calculated by the CWT method (bottom rows) with different dilation parameters (s).

5   Discussion

When applied to discrete data in the computer calculation, the CWT-based differentiation method can be equivalent to an LPDD[24]. The DWT-based method can also be regarded as an LPDD according to the implementation of Mallat's algorithm and A' trous algorithm[7, 10]. The filter lengths of the LPDDs corresponding to the CWT or DWT increase with the increasing dilation parameter or the decomposition level[22]. In Ref. [5], three properties of the LPDDs, i.e. the noise amplification factor, the minimum square-error and the optimum cut-off frequency, were successfully used to explain the results of different LPDDs, including the SNRe, the contrast, the CNRe and the AR. It is expected that the above three parameters can also be used to explain the results of the CWT or DWT method since both methods can be equivalent to specific LPDDs. The noise amplification factor, the minimum square-error and the optimum cut-off frequency will decrease with the in-

creasing dilation parameter or the decomposition level. Therefore, the noises will be eliminated more and thus the SNRe will be improved, at the expense of a reduced contrast and AR. The CNRe combines the behavior of the noise (or SNRe) and contrast[5,29,30]. Therefore, there exists a trade-off[5,29,30] for the selection of dilation parameter or decomposition level to obtain the highest CNRe.

The quadratic spline function was used as the wavelet function. However, other wavelet functions, e.g. the Haar wavelet function (equivalent to the db1, bior1.1 or sym1 function)[18,21,21], the derivative of the Gaussian smoothing function (Gaus1)[20,21] and the biorthogonal spline wavelet (bior1.1, bior1.3 and bior1.5)[21], could also be used as long as they have no more than one vanishing moment. The comparison of different wavelet functions and different dilation parameters or decomposition levels should be performed. Other than the CNRe, the SNRe, the contrast and the AR should be studied quantitatively[7]. In addition, comparison of the WT-based method and other methods[2,6,7] needs further investigation.

6　Conclusion

In this work, the axial strains in ultrasound elastography have been calculated from the estimated axial displacements using the WTs, including CWTs and DWTs. Computer simulations and some phantom data have validated the feasibility of this method. Results show that the WT-based method can greatly reduce the noises in axial strain calculation. However, further studies including the comparison of different parameters and different methods are needed.

References

1　Ophir J., Céspedes I., Ponnekanti H. et al. Elastography: A quantitative method for imaging the elasticity of biological tissues. Ultrason. Imaging, 1991, 13: 111—134.

2　O'Donnell M., Skovoroda A. R., Shapo B. M. et al. Internal displacement and strain imaging using ultrasonic speckle tracking. IEEE Trans. Ultrason. Ferroelectr. Freq. Control, 1994, 41: 314—325.

3　Konofagou E. E. Quo vadis elasticity imaging? Ultrasonics, 2004, 42: 331—336.

4　Orfanidis S. J., Introduction to Signal Processing. Englewood Cliffs, NJ: Prentice-Hall, 1996.

5　Usui S. and Amidror I. Digital low-pass differentiation for biological signal-processing. IEEE Trans. Biomed. Eng., 1982, 29: 686—693.

6　Kallel F. and Ophir J. A least-squares strain estimator for elastography. Ultrason. Imaging, 1997, 19: 195—208.

7　Luo J. W., Bai J., He P. et al. Axial strain calculation using a low-pass digital differentiator in ultrasound elastography. IEEE Trans. Ultrason. Ferroelectr. Freq. Control, 2004, 51: 1119—1127.

8　Bilgen M. Wavelet transform-based strain estimator for elastography. IEEE Trans. Ultrason. Ferroelectr. Freq. Control, 1999, 46: 1407—1415.

9　Alam S. K., Ophir J. and Konogagou E. E. An adaptive strain estimator for elastography. IEEE Trans. Ultrason. Ferroelectr. Freq. Control, 1998, 45: 461—472.

10　Mallat S. A Wavelet Tour of Signal Processing, 2nd ed. San Diego, CA: Academic Press, 1998.

11　Yang F. S. Engineering Analysis and Application of Wavelet Transform. Beijing: Science Press, 1999.

12　Mallat S. and Hwang W. L. Singularity detection and processing with wavelets. IEEE Trans. Inf. Theory, 1992, 38: 617—643.

13　Mallat S. and Zhong S. Characterization of signals from multiscale edges. IEEE Trans. Pattern Anal. Mach. Intell., 1992, 14: 710—732.

14　Mallat S. Zero-crossings of a wavelet transform. IEEE Trans. Inf. Theory, 1991, 37: 1019—1033.

15　Lee J. S., Sun Y. N. and Chen C. H. Multiscale corner detection by using wavelet transform. IEEE Trans. Image Process., 1995, 4: 100—104.

16　Li C. W., Zheng C. X. and Tai C. F. Detection of ECG characteristic points using wavelet transforms. IEEE Trans. Biomed. Eng., 1995, 42: 21—28.

17　Leung A. K. M., Chau F. T. and Gao J. B. Wavelet transform: A method for derivative calculation in analytical chemistry. Anal. Chem., 1998, 70: 5222—5229.

18　Shao X. G., Pang C. Y. and Su Q. D. A novel method to calculate the approximate derivative photoacoustic spectrum using continuous wavelet transform. Fresenius J. Anal. Chem., 2000, 367: 525—529.

19　Zhang S. L., Zheng J. B., Gu W. L. et al. Application of spline wavelet transform in differential of electroanalytical signal. Chin. Sci. Bull., 2001, 46: 550—555.

20　Nie L., Wu S. G., Lin X. Q. et al. Approximate derivative calculated by using continuous wavelet transform. J. Chem. Inf. Comput. Sci., 2002, 42: 274—283.

21　Shao X. G. and Ma C. X. A general approach to derivative calculation using wavelet transform. Chemometrics Intell. Lab. Syst., 2003, 69: 157—165.

22　Shao X. G. Application of wavelet transform in chemistry. in: Chemometrics: From Basics to Wavelet Transform. Hoboken, NJ: Wiley-Interscience, 2004.

23　Gentile A. and Messina A. On the continuous wavelet transforms applied to discrete vibrational data for detecting open cracks in damaged beams. Int. J. Solids Struct., 2003, 40: 295—315.

24　Messina A. Detecting damage in beams through digital differentiator filters and continuous wavelet transforms. J. Sound Vibr., 2004, 272: 385—412.

25　Bruce L. M. and Li J. Wavelets for computationally efficient hyperspectral derivative analysis. IEEE Trans. Geosci. Remote Sensing, 2001, 39: 1540—1546.

26　Chau F. T., Shih T. M., Gao J. B. et al. Application of the fast wavelet transform method to compress ultraviolet-visible spectra. Appl. Spectrosc., 1996, 50: 339—348.

27 Hayes J. W., Glover D. E., Smith D. E. et al. Some observations on digital smoothing of electroanalytical data based on the Fourier transformation. Anal. Chem., 1973, 45: 277—284.

28 Misiti M., Misiti Y., Oppenheim G. et al. Wavelet Toolbox for Use with MATLAB, User's Guide, Version 2. Natick, MA: The MathWorks Inc., 2002.

29 Varghese T., Ophir J., Konofagou E. et al. Tradeoffs in elastographic imaging. Ultrason. Imaging, 2001, 23: 216—248.

30 Srinivasan S., Righetti R. and Ophir J. Trade-offs between the axial resolution and the signal-to-noise ratio in elastography. Ultrasound Med. Biol., 2003, 29: 847—866.

31 Alam S. K., Ophir J. and Varghese T. Elastographic axial resolution criteria: An experimental study. IEEE Trans. Ultrason. Ferroelectr. Freq. Control, 2000, 47: 304—309.

32 Righetti R., Ophir J. and Ktonas P. Axial resolution in elastography. Ultrasound Med. Biol., 2002, 28: 101—113.

33 Bilgen M. Target detectability in acoustic elastography. IEEE Trans. Ultrason. Ferroelectr. Freq. Control, 1999, 46: 1128—1133.

34 Srinivasan S., Ophir J. and Alam S. K. Elastographic imaging using staggered strain estimates. Ultrason. Imaging, 2002, 24: 229—245.